

## Change of bulk and shear moduli of dry sandstone with effective pressure and temperature

John J. Zhang and Laurence R. Bentley

### ABSTRACT

The bulk and shear moduli of dry sandstone increase with effective pressure and decrease with temperature and the rate of change varies with effective pressure and temperature. In order to calculate the effect of effective pressure, a rock physics model based on pore aspect ratio spectra (KT model) is adopted in computation of elastic moduli and velocities. The pore aspect ratio spectra for a set of water-saturated sandstone samples are first assumed to be proportional to that of the standard sample, and are then adjusted to fit velocity measurements. Dry bulk and shear moduli at different pressures are calculated with the optimized pore aspect ratio spectra by setting the bulk moduli of contained fluid equal zero. It is found that the exponential relationship exists between the rate of change of elastic moduli and effective pressure as follows:

$$dK_d/dP = 0.746\exp(-0.0773P)$$

$$d\mu_d/dP = 0.372\exp(-0.0791P)$$

The effective pressure is between 5-40 MPa and the temperature at 22<sup>0</sup> C in laboratory. The temperature effect, which is due to pore volume change, is manifested as a more or less linear trend, and is modeled, based on experimental data, as straight lines:

$$dK_d/dT = -0.0155$$

$$d\mu_d/dT = -0.0065$$

The temperature ranges from 10 to 200<sup>0</sup> C and the effective pressure is from 25 to 500 MPa in laboratory.

### INTRODUCTION

Elastic moduli of dry rock vary as a function of effective pressure and temperature. Both bulk and shear moduli increase with effective pressure and decrease with temperature. The increase can be explained in terms of the closing of cracks and pores (Toksoz et al., 1976; Cheng et al., 1979; Walsh, 1965), whereas the decrease is largely due to pore volume change. As effective pressure increases, the cracks and flat pores of low aspect ratio close first, leading to a rapid increase in elastic moduli. At higher effective pressure, the spheroidal pores of high aspect ratio become thinner and close, but the rate of pore closing slows down due to the difficulty in the closing of these pores. As temperature increases, pore volume increases and the differential thermal expansion of minerals may cause cracks to open, decreasing elastic moduli.

In this paper, the KT model along with the expression of effective pressure dependence of elastic moduli is introduced. The pore aspect ratio spectra for 60

water-saturated sandstone samples (Han et al, 1986) are assumed to be proportional to that of the standard sample and are then adjusted to fit velocity measurements. The dry elastic moduli of these samples are subsequently calculated by setting the bulk modulus of contained fluid equal to zero. The slope of the dry elastic moduli with respect to effective pressure is modeled using an exponential function. For the effect of temperature, a more or less linear trend is found between temperature and dry elastic moduli based on experimental data.

### THEORETICAL MODELS

Nearly all rocks contain pores (Brace et al., 1972), which differ in shape from circular geometry to flat cracks and contacts (Cheng et al., 1979; Kowallis et al., 1984; Kuster and Toksoz, 1974; Sprunt and Brace, 1974; Timur et al., 1971; Toksoz et al., 1976). These pores of varying shape play a significant role in the determination of elastic moduli and wave velocities of rocks. Kuster and Toksoz (1974) propose a model to calculate elastic moduli based on pore geometry (pore aspect ratio spectrum). The model for spheroidal pores saturated with a fluid can be expressed as follows (Wang and Nur, 1991):

$$K = \frac{3K_s(3K_s + 4\mu_s) + 4\mu_s(K_f - K_s)A}{3(3K_s + 4\mu_s) - 3(K_f - K_s)A}$$

$$= \frac{25\mu_s^2(3K_s + 4\mu_s) - \mu_s^2(9K_s + 8\mu_s)B}{25\mu_s(3K_s + 4\mu_s) + 6\mu_s(K_s + 2\mu_s)B}$$

$$A = \sum_{n=1}^N C(a_n)T_{ijij}(a_n) \quad B = \sum_{n=1}^N C(a_n)[T_{ijij}(a_n) - \frac{1}{3}T_{ijij}(a_n)]$$

where  $a_n$  is the  $n$ th aspect ratio of the pores,  $C(a_n)$  is the volume fraction of  $a_n$ ,  $K_s$  and  $\mu_s$  are the bulk and shear moduli of the rock solid, respectively, and  $K_f$  is the bulk moduli of contained fluid, (expressions for  $T_{ijij}$  and  $T_{ijij}$  are given in Appendix A). The model for circular pores filled with a fluid can be expressed as:

$$K = \frac{4\mu_s C(K_f - K_s) + K_s(3K_f + 4\mu_s)}{(3K_f + 4\mu_s) - 3C(K_f - K_s)}$$

$$\mu = \frac{\mu_s(9K_s + 8\mu_s) - C\mu_s(9K_s + 8\mu_s)}{(9K_s + 8\mu_s) + 6C(K_s + 2\mu_s)}$$

where  $C$  is the volume fraction of circular pores. The model for the combination of circular pores and other pore shape is derived as:

$$K = \frac{-4\mu_s \left[ C \frac{K_f - K_s}{3K_f + 4\mu_s} + \frac{K_f - K_s}{3(3K_s + 4\mu_s)} A \right] - K_s}{3C \frac{K_f - K_s}{3K_f + 4\mu_s} + \frac{K_f - K_s}{3K_s + 4\mu_s} A - 1}$$

$$\mu = \frac{\mu_s - C\mu_s - \frac{\mu_s(9K_s + 8\mu_s)}{25(3K_s + 4\mu_s)} B}{1 + \frac{6C(K_s + 2\mu_s)}{9K_s + 8\mu_s} + \frac{6(K_s + 2\mu_s)}{25(3K_s + 4\mu_s)} B}$$

The assumptions involved in the derivation of the above equations are macrohomogeneity, isotropy and a dilute concentration of pores.

According to the model,  $K$  and  $\mu$ , then velocities, of a rock can be calculated when the pore aspect ratio spectrum and elastic moduli of rock solid and the bulk moduli of the contained fluid are known.

In order to model the changes in the elastic moduli (and therefore seismic velocities) of a rock as a function of pressure, the rate of crack closing with pressure must be calculated. Toksoz *et al.* (1976) give the following expression for the fractional change in the volume of pores of aspect ratio  $a$  and pressure  $P$ :

$$\frac{dC}{C} = \frac{-P}{K_A^*} / [E_1 - E_2 E_3 / (E_3 + E_4)]$$

where all the  $E_i$  are functions of the aspect ratio and some effective matrix moduli  $K_{IA}$  and  $\mu_{IA}$  defined as the effective moduli of the rock with all the pores except those with aspect ratio  $a$ .  $K_A^*$  is the static bulk modulus of the empty rock (Toksoz, et al., 1976), but because of the lack of such data it is usually taken to be the dynamic bulk moduli of the dry rock. The expression for  $E_i$  is given in appendix B. Given that the volume of a spheroid is represented by  $C=4\bullet R^3 a/3$ , with  $R$  as the radius of the spheroid, and assuming that changes in  $R$  are small, the following applies:

$$dC/C = da/a$$

The fractional rate of change of aspect ratio is therefore the same as that of the fractional change of porosity.

## DETERMINATION OF PORE ASPECT RATIO SPECTRA

Velocity measurements obtained in the laboratory yield important information about pore aspect ratio spectra. Laboratory data from previous work (Han *et al.*, 1986) are employed. These samples for velocity measurement were obtained from well cores or quarries, with porosities from 2 to 30% and clay content from 0 to 50%. Some are well-consolidated and others poorly-consolidated. These are considered to be representative of different kinds of sandstone. The  $V_p$  measurements of water-saturated samples with effective pressure from 5MPa to 40MPa are shown in Figure 1. The slope of velocity versus effective pressure is similar for samples considered. If some abnormal points are rejected, the  $V_p$  change from 5 MPa to 40 MPa is around 0.3 km/s for these samples. This implies that pore shapes are similarly distributed (Tosaya and Nur, 1982) and also that the velocity versus effective pressure of these dry samples may be parallel.

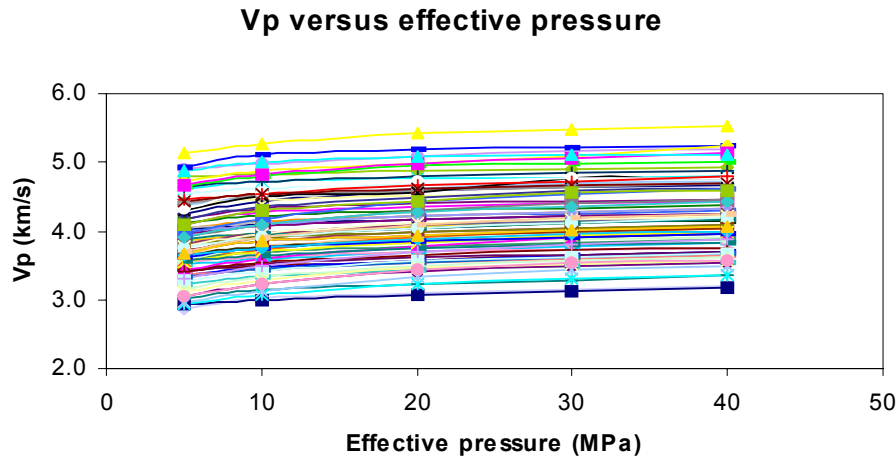


Figure 1.  $V_p$  versus effective pressure for sandstone samples

Calculation of the pore aspect ratio spectra from velocity measurements presents an inverse problem. Toksoz *et al.* (1976) and Cheng *et al.* (1979) obtained pore aspect ratio spectra of several rock samples from velocity measurements using inversion methods and found that volume fractions of pores with aspect ratio greater than  $10^{-4}$  could be determined uniquely and the maximum number of aspect ratios that could be resolved with the available data is around 10. Based on the conclusion and the possibility of similar distribution of pore shapes, the modified pore aspect ratio spectrum of Navajo sandstone is employed as a standard sample (Table 1). We assume any other sandstone of porosity  $\phi$  will have a pore aspect ratio distribution related to that of the standard sample according to the proportionality:

$$C_i(a_i)/C_i(a_i)^{standard} = \phi/\phi^{standard},$$

where  $C_i$  is the volume fraction of pores of aspect ratio  $a_i$ . In other words, the pore geometry of any sandstone is a scaled replica of the standard sample's.

Table 1. Pore aspect ratio spectrum of Navajo sandstone (after Cheng *et al.*, 1979)

$a_i$	$C_i$	$a_i$	$C_i$	$a_i$	$C_i$
1	0.1416	0.0028	0.0002	0.0009	0.000065
0.1	0.0210	0.0021	0.00015	0.0006	0.00011
0.01	0.00024	0.0016	0.00018	0.0003	0.00011
0.0035	0.00014	0.0012	0.00014	0.0001	0.00001

$$\phi = 16.41 \%, K_s = 34 \text{ GPa}, \mu_s = 26 \text{ GPa}$$

The pore aspect ratio spectra obtained above are further adjusted to fit velocity measurements. Figures 2, 3, 4, and 5 are examples of the results. The average error bar from the fitting for 60 water-saturated samples is  $\pm 0.0646$  km/s. The adjusted aspect ratio spectra of the four samples are presented in Tables 2, 3, 4 and 5.

The adjusted pore aspect ratio spectra of 60 samples were used to calculate the corresponding dry elastic moduli and velocities of these samples by setting  $K_f$  equal 0. As shown in Figures 2, 3, 4 and 5, the slope of dry velocity versus effective pressure is steeper than that of wet velocity, especially at low effective pressure, due to the existence of cracks. At higher effective pressure, dry velocities come close to, and even exceed, wet velocities due to the end of crack closing.

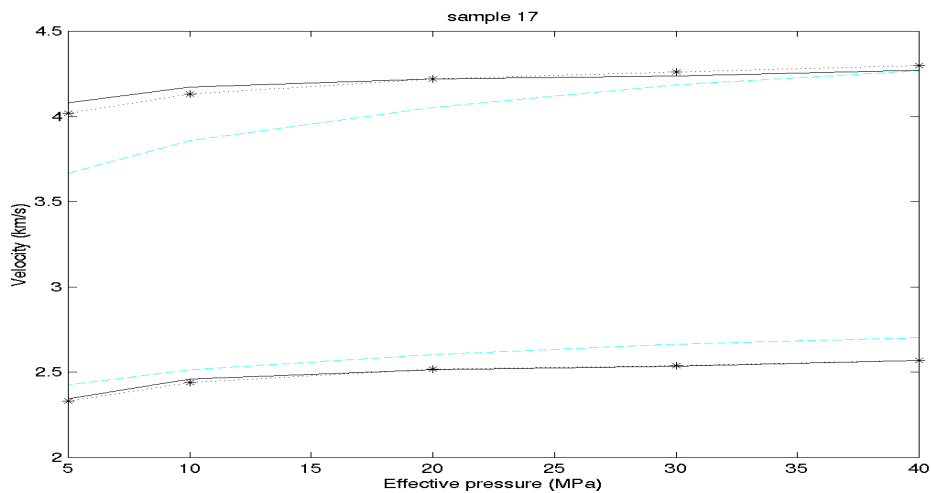


Figure 2. Velocities versus effective pressure for sample 17. Dashed blue lines denote calculated dry velocities, solid black lines denote calculated water-saturated velocities and dotted lines with \* denote laboratory-measured water-saturated velocities. Upper curves are compressional wave, and lower curves are shear wave.

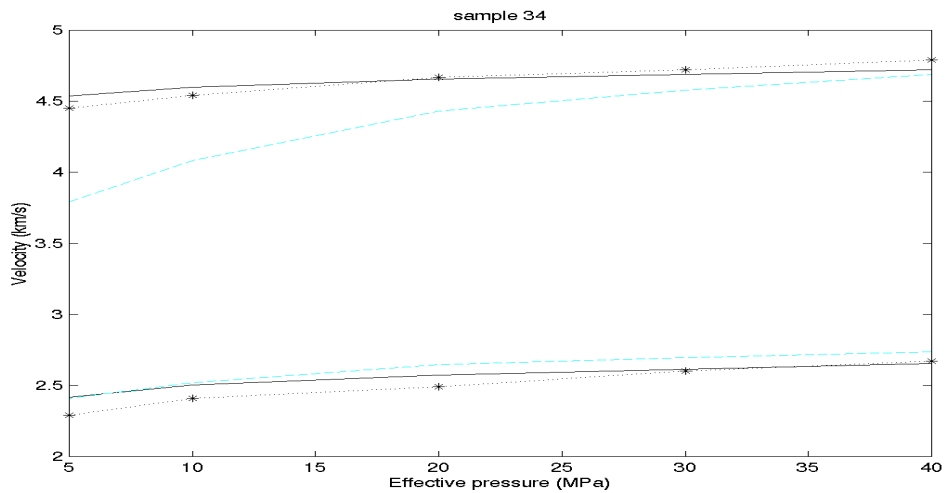


Figure 3. Velocities versus effective pressure for sample 34. Dashed blue lines denote calculated dry velocities, solid black lines denote calculated water-saturated velocities and dotted lines with \* denote laboratory-measured water-saturated velocities. Upper curves are compressional wave and lower curves are shear wave.

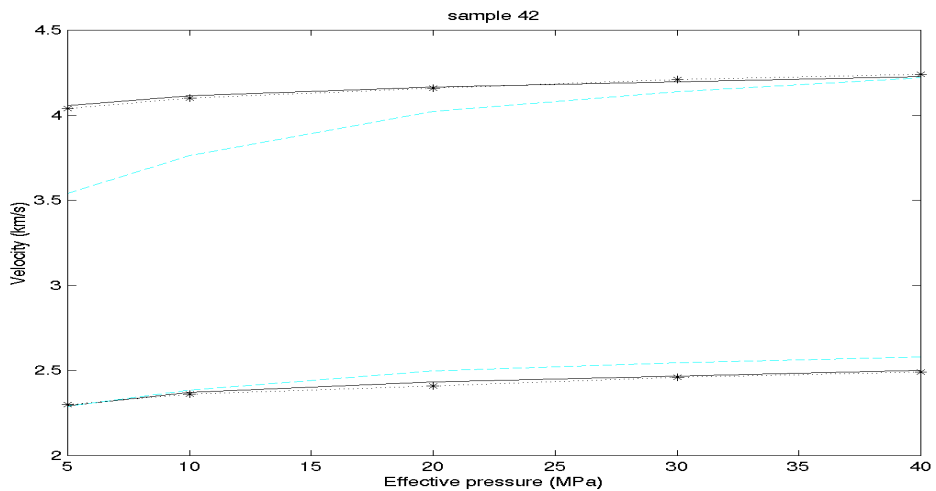


Figure 4. Velocities versus effective pressure for sample 42. Dashed blue lines denote calculated dry velocities, solid black lines denote calculated water-saturated velocities and dotted lines with \* denote laboratory-measured water-saturated velocities. Upper curves are compressional wave and lower curves are shear wave.

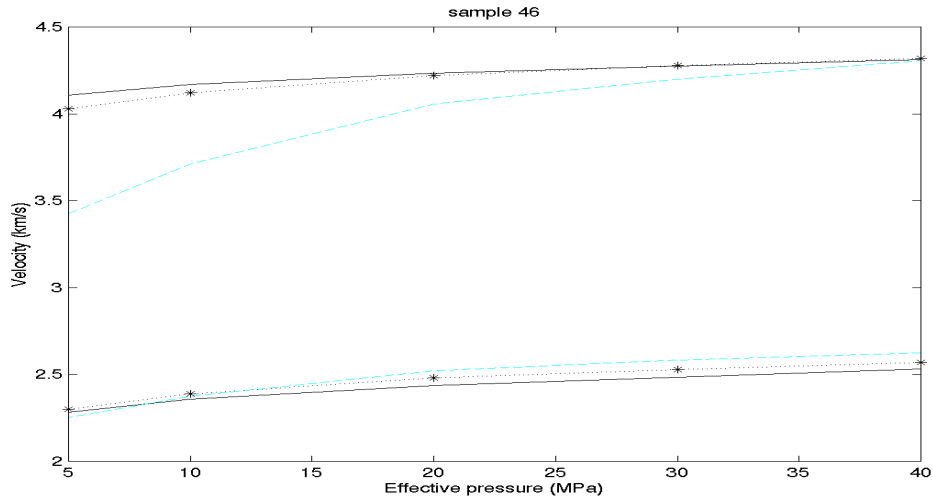


Figure 5. Velocities versus effective pressure for sample 46. Dashed blue lines denote calculated dry velocities, solid black lines denote calculated water-saturated velocities and dotted lines with \* denote laboratory-measured water-saturated velocities. Upper curves are compressional wave and lower curves are shear wave.

Table 2. Pore aspect ratio spectrum of sample 17

$a_l$	$C_l$	$a_l$	$C_l$	$a_i$	$C_i$
1	0.1549	0.0028	0.00021	0.0009	0.000053
0.1	0.0236	0.0021	0.00015	0.0006	0.00010
0.01	0.00027	0.0016	0.00018	0.0003	0.00011
0.0035	0.00014	0.0012	0.00014	0.0001	0.000013

$$\phi = 17.98 \%, K_s = 33 \text{ GPa}, \mu_s = 26 \text{ GPa}$$

Table 3. Pore aspect ratio spectrum of sample 34

$a_l$	$C_l$	$a_l$	$C_l$	$a_i$	$C_i$
1	0.0709	0.0028	0.00019	0.0009	0.00013
0.1	0.0000084	0.0021	0.00017	0.0006	0.00015
0.01	0	0.0016	0.00018	0.0003	0.000088
0.0035	0.00016	0.0012	0.00016	0.0001	0.000049

$$\phi = 7.22 \%, K_s = 28 \text{ GPa}, \mu_s = 22 \text{ GPa}$$

Table 4. Pore aspect ratio spectrum of sample 42

$a_i$	$C_i$	$a_i$	$C_i$	$a_i$	$C_i$
1	0.0775	0.0028	0.00018	0.0009	0.00011
0.1	0.00051	0.0021	0.00015	0.0006	0.00013
0.01	0	0.0016	0.00017	0.0003	0.000082
0.0035	0.00015	0.0012	0.00015	0.0001	0.00004

$$\phi = 7.92 \%, K_s = 28 \text{ GPa}, \mu_s = 20 \text{ GPa}$$

Table 5: Pore aspect ratio spectrum of sample 46

$a_i$	$C_i$	$a_i$	$C_i$	$a_i$	$C_i$
1	0.0823	0.0028	0.00021	0.0009	0.00015
0.1	0	0.0021	0.00019	0.0006	0.00017
0.01	0	0.0016	0.00020	0.0003	0.000081
0.0035	0.00019	0.0012	0.00019	0.0001	0.000039

$$\phi = 8.37 \%, K_s = 30 \text{ GPa}, \mu_s = 21 \text{ GPa}$$

### CHANGE OF ELASTIC MODULI WITH EFFECTIVE PRESSURE

The dry elastic moduli of the 60 samples evaluated above are differentiated with respect to effective pressure at a series of effective pressure points with the results plotted in Figures 6 and 7. An exponential function was found to best represent the data as follows.

$$dK_d/dP = 1.047\exp(-0.1356P) \quad (1)$$

$$d\mu_d/dP = 0.459\exp(-0.1206P) \quad (2)$$

The major uncertainty for these two equations arises from high values at low effective pressure. Another problem is that the two equations are much lower than the majority of data points at 20-40 MPa, although they are best fitting. To solve these problems, the derivatives of 60 samples at each effective pressure point are averaged, and the other two regression equations are obtained as follows.

$$dK_d/dP = 0.789\exp(-0.0612P) \quad (3)$$

$$d\mu_d/dP = 0.387\exp(-0.0644P) \quad (4)$$

Equations (3) and (4) rectify the two problems of equations (1) and (2), but are slightly large at high effective pressure. A compromise can be reached by averaging the two equations for bulk and shear moduli respectively and providing the following relationship:

$$dK_d/dP = 0.746\exp(-0.0773P) \quad (5)$$

$$d\mu_d/dP = 0.372\exp(-0.0791P) \quad (6)$$

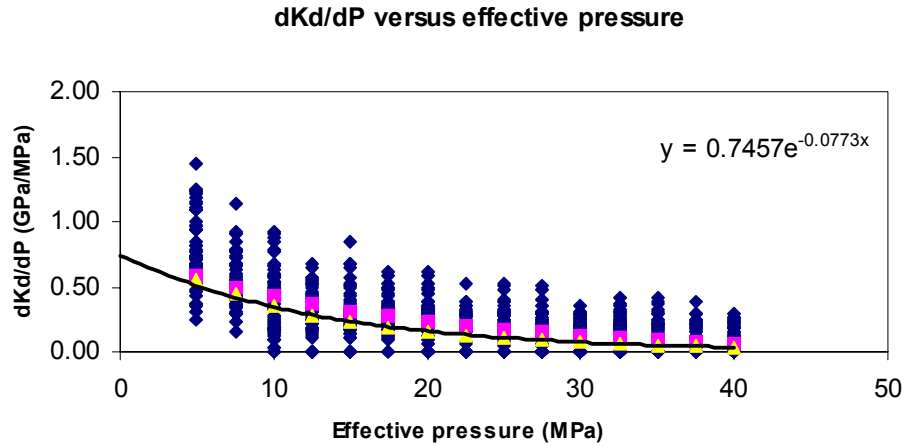


Figure 6. Slope of bulk moduli versus effective pressure for 60 samples

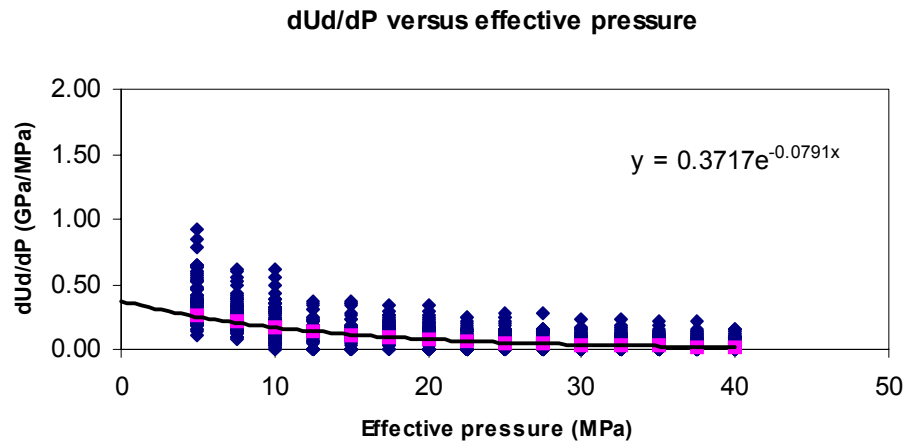


Figure 7. Slope of shear moduli versus effective pressure for 60 samples

In order to test the validity of these regression lines, velocity and elastic modulus measurements in laboratory are compared with the results calculated from the above equations. Gregory (1976) makes a series of velocity and density measurements for a group of rocks including sand and sandstone. Table.3 in his paper lists  $V_p$ ,  $V_s$  and elastic moduli for the Gulf Coast sand. Table 6 shows the test results, which include laboratory measurements and those calculated with Equations 5 and 6.

Table 6. Dry elastic moduli at different pressures for the Gulf Coast sand (laboratory measurements versus calculations from our equations)

Pressure (MPa)	Measured $K$ (GPa, Gregory, 1976)	Calculated $K$ (Gpa)	Error	Measured $\mu$ (Gpa, Gregory, 1976)	Calculated $\mu$ (GPa)	Error
0	2.8983	2.8983	0	6.9808	6.9808	0
3.4	3.6280	5.1288	1.50	7.2686	8.0888	0.82
6.8	4.9728	6.8439	1.87	7.5843	8.9356	1.35
13.6	7.8438	9.1757	1.33	8.5360	10.0773	1.54
20.4	9.1888	10.5553	1.36	9.7328	10.7439	1.01
27.2	10.3319	11.3705	1.03	10.6481	11.1333	0.48
34	10.9787	11.8500	0.87	11.3814	11.3606	-0.02
40.8	11.5779	12.1373	0.55	11.8966	11.4934	-0.40
47.6	11.9879	12.3057	0.31	12.3306	11.5710	-0.76
54.4	12.3671	12.4053	0.04	13.6943	11.6162	-2.07
61.2	12.6176	12.4641	-0.15	12.9844	11.6427	-1.34
68	12.7857	12.4990	-0.28	13.2136	11.6581	-1.55

The measured bulk and shear moduli at  $P=0$  are used as the starting values. The values in the column ‘Calculated’ are calculated as follows:

$$K_{dn} = -9.651[\exp(-0.0773P_n)-1] + K_{d0} \quad (7)$$

$$\mu_{dn} = -4.699[\exp(-0.0791P_n)-1] + \mu_{d0} \quad (8)$$

where  $K_{dn}$  and  $\mu_{dn}$  are the bulk and shear moduli at the  $n$ th pressure point  $P_n$  (e.g.,  $n=1$ ,  $P=3.4$ MPa), and  $K_{d0}$  and  $\mu_{d0}$  are the bulk and shear moduli at zero pressure.

The average error bar between measured and calculated values is  $\pm 1.11$  (GPa). The major source of error may be due to experimental error. For example, the shear modulus decreases with increasing effective pressure between  $P=54.4$  and  $P=61.2$  MPa, and the slope of the experimental bulk moduli reverses between  $P=3.4$  and  $P=6.8$  MPa. Our figures seem more reasonable.

Berea sandstone is a classical sandstone for rock physics study. Its velocities were read from Cheng’s paper (1979, Figure 1) and are listed in Table 7, which also includes the elastic modulus results. The porosity of Berea sandstone is 0.163 and the density of its rock solid is assumed 2.7 gm/cm<sup>3</sup>. The density is calculated as  $(1-16.3\%)*2.7$ .

Table 7. Dry velocities and elastic moduli for Berea sandstone

Pressure (MPa)	Density (kg/cm <sup>3</sup> )	$V_p$ (km/s)	$V_s$ (km/s)	$K$ (GPa)	$\mu$ (GPa)	Calculated $K$ (GPa)	Calculated $\mu$ (GPa)
5	2.26	3.8	2.4	15.3	13	15.3	13
10	2.26	4.0	2.53	16.7	14.6	17.4	14.0
15	2.26	4.1	2.6	17.6	15.3	18.8	14.7
20	2.26	4.15	2.65	17.8	15.8	19.8	15.2
25	2.26	4.2	2.67	18.4	16.1	20.5	15.5
30	2.26	4.23	2.71	18.4	16.6	20.9	15.7
40	2.26	4.25	2.72	18.5	16.72	21.4	16.0
50	2.26	4.27	2.725	18.83	16.78	21.6	16.1

The calculation starts at  $P=5$  MPa. The average error bar between measured and calculated values is  $\pm 1.59$ (GPa), which is greater than that for Gregory's samples. The discrepancy may be due to the inaccurate reading of the velocity from the figures and the inaccurate calculation of density.

In all, the relationship of the slope of elastic moduli with respect to effective pressure is sufficiently accurate to enable the computing of the change of elastic moduli with an error bar within  $\pm 1.6$  GPa. The steeper slope at lower pressure in the relationship results from the fact that no experimental data are available at zero or very low pressure, a problem that will be considered in future research.

### CHANGE OF ELASTIC MODULI WITH TEMPERATURE

Temperature affects elastic moduli of a rock by changing the elastic moduli of the rock solid (e.g. quartz and clay) and its pore aspect ratio spectrum. The former is negligibly small (Carmichael, 1989) and will not be considered. The latter plays a significant role. When temperature increases, pore volume increases (even if the magnitude is small) and differential thermal expansion of the constitute minerals may cause new cracks to open (Hellwege, 1982), especially at grain boundaries. The opening of cracks occurs whenever temperature increases at a rate higher than  $100^{\circ}\text{C}/100\text{MPa}$  at high temperature (Kern, 1978). Below  $200^{\circ}\text{C}$ , however, the experimental data (Wang and Nur, 1988; Carmichael, 1989) do not observe the opening of cracks, a non-linear event. Therefore, with the exception of extreme thermal event such as those associated with steam flooding, the change of elastic moduli with temperature is attributable to the pore volume change, a linear event.

In order to find the slope of the straight line, velocity measurements and their change with temperature are collected. Carmichael's (1989) data for dry sandstone are plotted in Figures 8 and 9, which show a linear trend for the bulk and shear moduli. The slope can be approximated as:

$$dK_d/dT = -0.0155 \quad (9)$$

$$d\mu_d/dT = -0.0065 \quad (10)$$

The above equations are used to calculate elastic moduli in order to assess whether or not the error is reasonable. Wang and Nur (1988) measure a series of velocities at different temperatures. Table 8 shows the measured versus calculated values.

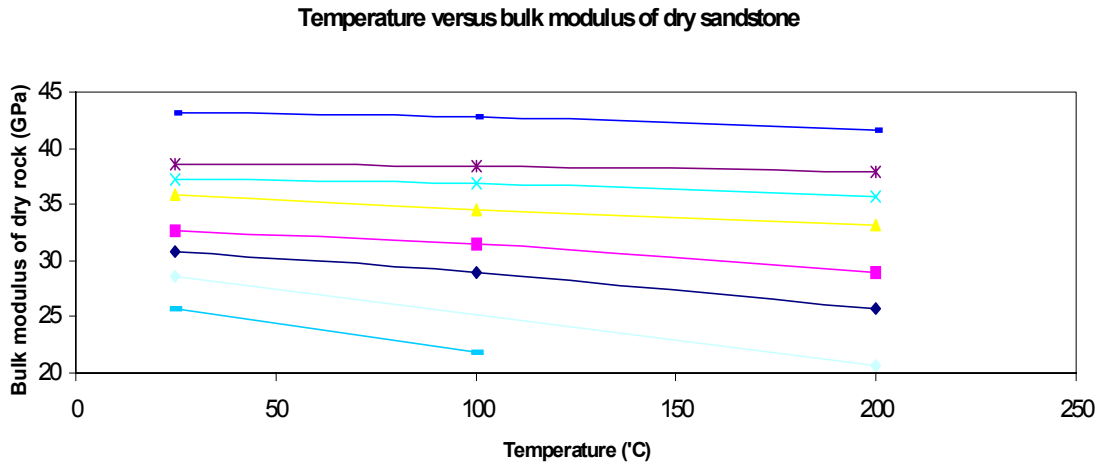


Figure 8. Bulk moduli versus temperature for sandstone (after Carmichael, 1989)

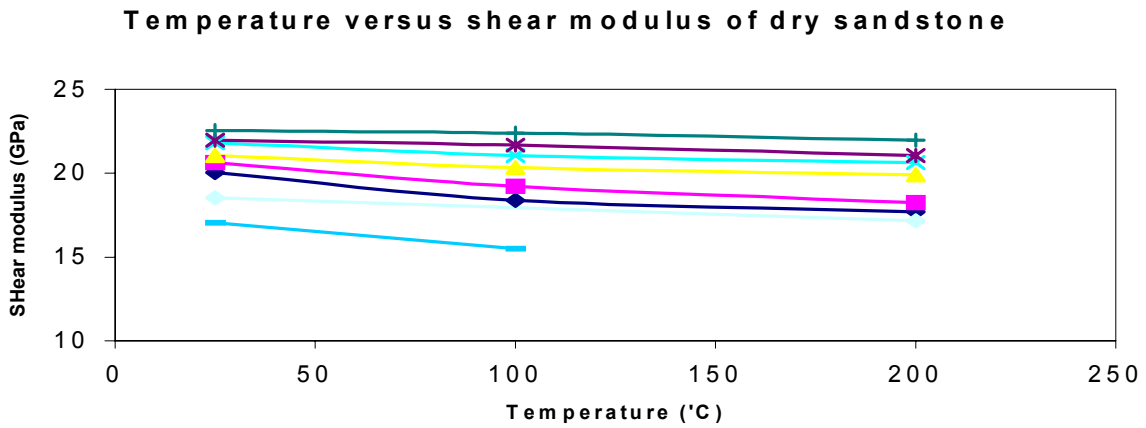


Figure 9. Shear moduli versus temperature for sandstone (after Carmichael, 1989)

Table 8. Dry velocities and elastic moduli for Massillon sandstone

$T$ (°C)	Density (kg/cm <sup>3</sup> )	$V_p$ (km/s)	$V_s$ (km/s)	$K$ (GPa)	$\mu$ (GPa)	Calculated $K$ (GPa)	Calculated $\mu$ (GPa)
20	2100	3.08	2.16	6.87	9.79	6.87	9.79
30	2100	3.06	2.14	6.84	9.62	6.72	9.72
40	2100	3.04	2.12	6.82	9.44	6.57	9.66
50	2100	3.00	2.11	6.43	9.35	6.42	9.59
60	2100	2.99	2.10	6.42	9.26	6.27	9.53
80	2100	2.98	2.09	6.42	9.17	5.97	9.40
100	2100	2.95	2.08	6.17	9.08	5.67	9.20
120	2100	2.94	2.05	6.39	8.82	5.37	9.14

The error is small. The change in bulk and shear moduli with temperature is also small. In the case of Massillon sandstone, 7% and 10% changes for bulk and shear moduli respectively occur at 100°C change in temperature.

### CONCLUSION

The KT rock physics model was used to calculate elastic moduli and velocities. The theory is based on the assumption that elastic moduli of a rock are determined by its pore aspect ratio spectrum, the elastic moduli of the rock solid and the bulk modulus of the pore fluid. With the model, the pore aspect ratio spectra of 60 water-saturated samples were estimated using velocity measurements. Then the pore aspect ratio spectra were used to calculate the dry bulk and shear moduli and velocities of the dry rock.

The dry bulk and shear moduli of 60 samples at different pressures were used to determine exponential relationships for the change in bulk modulus with respect to effective pressure and the change in shear modulus with respect to effective pressure. The relationships were validated using independent measurements on the Gulf Coast sand and Berea sandstone.

The bulk and shear moduli were found to decrease linearly with temperature below 200°C. The temperature effect is minimal.

## REFERENCES

- Brace, W. F., E. Silver, K. Hadley and C. Goetze, 1972, Cracks and pores: A closer look: *Science*, **168**, 162-163.
- Carmichael, Robert S., 1989, *Practical Handbook of Physical Properties of Rocks and Minerals*: CRC Press.
- Cheng, Chuen Hon and M. Nafi Toksoz, 1979, Inversion of seismic velocities for the pore aspect ratio spectrum of a rock: *Journal of Geophysical Research*, **84**(B13), 7533-7543.
- Gregory, A. R., 1976, Fluid saturation effects on dynamic properties of sedimentary rocks: *Geophysics*, **41**, 895-921
- Han, De-hua, A. Nur and Dale Morgan, 1986, Effects of porosity and clay content on wave velocities in sandstones: *Geophysics*, **51**, 2093-2107.
- Hellwege, K-H, 1982, *Physical properties of rocks*: Springer-Verlag Berlin-Heiddberg, volume **1**
- Kern, H., 1978, The effect of high temperature and high confining pressure on compressional wave velocities in quartz-bearing and quartz-free igneous and metamorphic rocks, *Tectonophysics*, **44**, 185-203.
- Kowallis, B. J., L. E. A. Jones and H. F. Wang, 1984, Velocity-porosity-clay content systematics of porosity consolidated sandstones: *Journal of Geophysical Research*, **89**(B12), 10355-10364.
- Kuster, Guy T. and M. Nafi Toksoz, 1974, Velocity and attenuation of seismic waves in two-phase media: part 1: *Geophysics*, **39**, 587-606.
- Sprunt, Eve S. and W. F. Brace, 1974, Direct observation of microcavities in crystalline rocks: *Int. J. Rock Mech. Min. Sci. Geomech., Abstr.*, **11**, 139-150.
- Timur, A., W. B. Hemphkins and R. M. Weinbrandt, 1971, Scanning electron microscopic study of pore systems in rocks: *Journal of Geophysical Research*, **76**(20), 4932-4948.
- Toksoz, M. N., C. H. Cheng and A. Timur, 1976, Velocities of seismic waves in porous rocks: *Geophysics*, **41**, 621-645.
- Tosaya, Carol and Amos Nur, 1982, Effects of diagenesis and clays on compressional velocities in rocks: *Geophysical Research Letters*, **9**(1), 5-8.
- Walsh, J. B., 1965, The effect of cracks on the compressibility of rock: *Journal of Geophysical Research*, **70**, 381-389
- Wang, Z. and A. M. Nur, 1988, Effect of temperature on wave velocities in sands and sandstones with heave hydrocarbons: *SPE Reservoir Engineering*, **3**(1) 158-164.
- Wang, Z. and A. M. Nur, 1991, *Seismic and Acoustic Velocities in Reservoir Rocks: Theoretical and Model Studies*, Society of Exploration Geophysicists, Volume **2**, 19-20.

**Appendix A**

$$T_{ijij} = \frac{3F_1}{F_2}$$

$$T_{ijij} - \frac{1}{3}T_{ijij} = \frac{2}{F_3} + \frac{1}{F_4} + \frac{F_4F_5 + F_6F_7 - F_8F_9}{F_2F_4}$$

where

$$F_1 = 1 - [3/2(g+\theta) - R(3/2g + 5/2\theta - 4/3)]$$

$$F_2 = 1 - [1 + 3/2(g+\theta) - R/2(3g + 5\theta)] + B(3 - 4R) - 1/2(3B - 1)(3 - 4R)(g + \theta - R(g - \theta + 2\theta^2))$$

$$F_3 = 1 - 1/2(R(2 - \theta) + (1 + a^2)/a^2g(R - 1))$$

$$F_4 = 1 - 1/4[3\theta + g - R(g - \theta)]$$

$$F_5 = B\theta(3 - 4R) - R(g + \theta - 4/3) + g$$

$$F_6 = B(1 - \theta)(3 - 4R) - g + R(g + \theta)$$

$$F_7 = 2 - 1/4[9\theta + 3g - R(5\theta + 3g)] + B\theta(3 - 4R)$$

$$F_8 = B(1 - \theta)(3 - 4R) - 1 + 2R - g/2(R - 1) - \theta/2(5R - 3)$$

$$F_9 = B\theta(3 - 4R) - g(R - 1) + R\theta$$

$$B = 1/3 K_f/K_s$$

$$R = 3\mu_s/(3K_s + 4\mu_s)$$

$$\theta = a/[(1 - a^2)^{3/2}](\cos(a) - a(1 - a^2)^{0.5})$$

$$g = a^2/(1 - a^2)(3\theta - 2)$$

**Appendix B**

$$E_1 = \frac{6 I A^I}{2 (3K_{1A} + 4 I A)}$$

$$E_2 = \frac{6 I A}{4\pi(3K_{1A} + 4 I A)} (3I - 4)$$

$$E_3 = \frac{a^2 (3 - 9I/4\pi - 6K_{1A} + 2 I A)}{2(1 - a^2)(3K_{1A} + 4 I A)} + \frac{6 I A^I}{8 (3K_{1A} + 4 I A)}$$

$$E_4 = \frac{1}{2} \left\{ \frac{(3 - 9I/4\pi)(6K_{1A} + 2 I A)}{2(1 - a^2)(3K_{1A} + 4 I A)} - \frac{3 I A^{(1-I)}}{(3K_{1A} + 4 I A)} \right\}$$

$$I = \frac{2 a}{(1 - a^2)^{3/2}} \{ \cos^{-1} a - a(1 - a^2)^{1/2} \}$$